ACS Sustainable Chemistry & Engineering

pubs.acs.org/journal/ascecg

Research Article

Amphiphilic Co-Solvents Modulate the Structure of Membrane Domains

Luoxi Tan, Haden L. Scott, Micholas Dean Smith, Sai Venkatesh Pingali, Hugh M. O'Neill, Jennifer L. Morrell-Falvey, John Katsaras, Jeremy C. Smith, Brian H. Davison, James G. Elkins, and Jonathan D. Nickels*

Cite This: *ACS Sustainable Chem. Eng.* 2023, 11, 1598–1609

Read Online

ACCESS | Metrics & More | Article Recommendations | Supporting Information

ABSTRACT: Biofuels are an increasing part of the sustainable energy picture. This makes it a societal and economic imperative to optimize biofuel production. Mitigating the toxic effects of amphiphilic co-solvents is one way to improve the efficiency of biofuel production. Amphiphiles partition into cellular membranes, leading to membrane thinning, destabilization, loss of membrane potential, and, ultimately, cell death. However, this picture of solvent toxicity misses the disruptive impact of co-solvents on lateral membrane organization, which is increasingly recognized as critical for membrane protein sorting and oligomerization. The alteration or disruption of membrane domains has deleterious effects on cellular processes. In this work, we pursue the hypothesis that membrane lateral organization is disrupted by the presence of co-solvents at concentrations lower than those which lead to full membrane destabilization. The disruption occurs due to an increasing interfacial tension between the co-existing phases, resulting in conformational changes to minimize the interfacial length-to-area ratio. This represents an unrecognized mode of solvent-induced stress and a new target for interventions to improve fermentation yields.

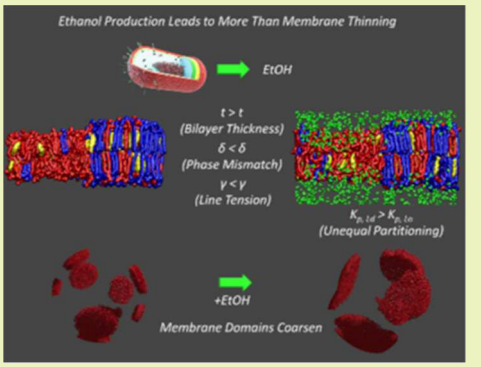

KEYWORDS: *biofuels, lipid phase behavior, neutron scattering, and molecular dynamics simulations*

INTRODUCTION

Amphiphilic co-solvents affect cells in a variety of ways, with the main impacts characterized as membrane interactions, allosteric effects on proteins, and broad metabolic changes which reallocate cellular resources.[1−3] Here, we take a deeper look at the phenomena behind the first, and indeed the most critical, of these: the membrane effects.[4,5] Amphiphilic co-solvent partitioning into cell membranes thins the structure and increases membrane fluidity.[4,6,7] As the concentration of the co-solvent increases, so does the passive proton flux.[8] This leads to a loss of the electrochemical gradient across the cell membrane[9] and results in the loss of ATPase activity.[10] This is ultimately fatal to the cell.

We focus on the physical effects of co-solvent partitioning at concentrations below those that impact the membrane potential directly via the above mechanism. Specifically, we investigate co-solvent partitioning in the context of lateral organization in lipid bilayers. Lateral organization is directly related to the notion of lipid rafts or functional membrane microdomains (FMMs). FMMs are regions of the cell membrane with distinct compositions and physical properties which act as platforms for the efficient oligomerization of interacting proteins.[11] An exemplary study showing the relevance of FMMs to function is the work of Lopez and Kolter,[12] which showed that lateral organization of the membrane protein organization could be disrupted by interference with the production of squalene-derived lipids. These squalene derivatives are thought to be enriched in membrane domains and to act in a role somewhat analogous to cholesterol in mammalian membranes. This connection has long been understood for mammalian membranes, dating back to detergent resistance studies and observations[13] of lateral demixing of lipids in apical membranes.[14] Subsequent work[15] has shown the functional impacts of FMM disruption.

The world is looking for new energy sources, and sustainably sourced biofuels have long been identified as part of the solution. Optimizing the yield of these biofuels and other bioproducts is an imperative if we wish to fully realize their potential. Amphiphilic co-solvents, such as alcohols or other fermentation products, induce significant stress on microbial cell membranes (or cells of the gastrointestinal lining) as described above. A potential nexus exists between fermentation

Received: November 16, 2022
Revised: January 4, 2023
Published: January 18, 2023

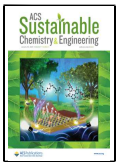

https://doi.org/10.1021/acssuschemeng.2c06876
ACS Sustainable Chem. Eng. 2023, 11, 1598–1609

yield and FMM disruption via the effect of domain disruption on the shared regulatory element, Spo0A. Spo0A is involved in the onset of both solvent production and sporulation. There is a limited duration and active solvent productivity of a cell as it progresses toward sporulation, raising the possibility that yields could be improved if active solvent production was decoupled from the onset of sporulation or if the onset of sporulation was delayed. The FMM associated proteins, Flotillin (FloA and FloT) and histidine kinase (KinC),[11,16] are involved in the phosphorylation of Spo0A.[17] This activity was reported to be lost upon the disruption of FMMs.[17] Indeed, a single knockout related to Spo0A was able to abort sporulation at the initiation stage and enhance butanol yield and tolerance in *Clostridium acetobytylicum*.[18]

The physical basis for lateral phase separation in lipid membranes can be described in terms of minimizing the total energy of a vesicle,[19] simplifying the case to a two-component (A and B) system in which a fixed number of molecules N_A and N_B comprise the surface, which itself consists of two coexisting phases (S, surround and D, domain). The total area fractions, A^S and A^D, of the two phases can be defined with the constraint

$$A^S\rho^S + A^D\rho^D = N_A + N_B \tag{1}$$

where ρ^i is the number density difference, defined as $\rho^i = \rho_A{}^i - \rho_B{}^i$, given that ρ_A and ρ_B are the number density per unit area of each component in a given phase, i. We can then define the total free energy of a vesicle, F, as

$$F = F_m + F_b + F_G \tag{2}$$

where F_b and F_G represent the normal and Gaussian bending energies, which can be further expanded. The term F_m represents the energy of the binary mixture

$$F_m = A^S f^S + A^D f^D + F_l \tag{3}$$

where f^i is the free energy density of the given phase, and F_l represents the energy of the domain boundary. The boundary energy can be described as

$$F_l = \gamma \int_{\partial D} dl \tag{4}$$

where γ is the line tension which represents the energetic penalty per length, integrated around the domain boundary, ∂D, of length, l. Kuzmin et al.[20] have developed a relationship to describe γ for a monolayer as

$$\gamma = \frac{\sqrt{B_S K_S B_D K_D}}{\sqrt{B_D K_D} + \sqrt{B_S K_S}} \frac{\delta^2}{h_0{}^2} - \frac{1}{2} \frac{(B_S J_S - B_D J_D)^2}{\sqrt{B_D K_D} + \sqrt{B_S K_S}} \tag{5}$$

where δ is the monolayer thickness mismatch between the domain and surround, h_0 is the average monolayer thickness, B_i is the bending modulus, K_i is the tilt modulus, and J_i is the spontaneous curvature.

Leveraging this physical understanding of lipid phase behavior, our study contextualizes observed changes in lipid domain size due to the partitioning of the amphiphilic co-solvent, ethanol (EtOH). The fundamental mechanism by which solvent partitioning leads to coarsening of lipid domains is tied to an increase of the line tension.[21] We use small-angle neutron scattering (SANS) to interrogate the effect of ethanol on the morphology of lipid domains in a well-studied family of phase-separating model lipid mixtures.[22−25] After demonstrating the increase in domain size using SANS, we characterize the structure of the individual phases using a combination of additional SANS experiments and atomistic molecular dynamics (MD) simulations in terms of bilayer thickness, partition coefficient, and mechanical properties. These analyses reveal preferential partitioning of EtOH into the liquid disordered (Ld) phase—relative to the co-existing liquid ordered (Lo) phase. This leads to an increase in the thickness mismatch between the two phases, resulting in an increased line tension between the phases as evaluated by eq 5. Increased line tension favors a decrease in the ratio of interfacial length to domain area—leading to fewer, larger domains.

RESULTS AND DISCUSSION

EtOH Addition Coarsens Lipid Domains. The effect of ethanol (EtOH) on nanoscopic domains was observed using SANS in small unilamellar vesicle (SUV) samples. These SUVs were produced from a family of phase-separating lipid mixtures composed of 1-palmitoyl-2-oleoyl-*glycero*-3-phosphocholine (POPC), 1,2-dioleoyl-*sn*-glycero-3-phosphocholine (DOPC), and 1,2-distearoyl-*sn*-glycero-3-phosphocholine (DSPC). This is an archetypical high-melting lipid/low-melting lipid/cholesterol system,[22] with DSPC being the high-melting lipid and POPC and/or DOPC representing the low-melting lipid. A selection of seven phase-separating lipid mixtures was constructed with a systematic increase in the fraction of DOPC in the low-melting lipid component. Borrowing the nomenclature from Heberle et al.,[25] we will refer to these samples as D1 (POPC/DSPC/Chol.) to D7 (DOPC/DSPC/Chol.); see Table S1 for details. In varying the ratio of the low-melting lipid from POPC to DOPC, the domain size can be controllably varied—a phenomenon tied to changes in the line tension.[21,25] This mixture is considered a model mammalian cell membrane mimic and has been well characterized in terms of the tie lines.[22−26] Thus, the compositions of the individual coexisting phases[26] are known; see Table S2. This allowed Heberle et al.[25] to develop an isotopic labeling strategy to enable a de-mixing experiment based on viable neutron scattering length density (SLD).

Figure 1A illustrates the concept of a SANS-based de-mixing experiment. Contrast variation and contrast matching are key concepts for this type of SANS experiment.[27] Neutrons scatter from the SLD, a quantity which varies by element and isotope. Contrast variation is then the systematic change of the SLD typically based on the controlled substitution of natural abundance hydrogen (H) with its isotope ^{2}H or deuterium (D) in the bilayer or solvent. Neutrons scatter quite differently from these isotopes, resulting in control of the SLD profile without changing the structure. Contrast matching is the condition achieved when the solvent and the vesicle have the same SLD, and no scattering from the vesicle is observed. The de-mixing experiment leverages this by creating an SUV which, if homogeneously mixed, will match the SLD of the solvent and result in a null-scattering condition. Yet if phase separation occurs, the component lipids will be distributed inhomogeneously, and local H/D content (and SLD) will no longer reflect the average value—resulting in observable scattering, as seen in Figure 1B. Here, we produced SUV samples with a mixture of tail-deuterated (D) lipids and "normal" hydrogenated (H) lipids in such a way that the average neutron SLD of the hydrophobic portion of the lipid bilayer matches that of the PC headgroup (0.181 fm/Å^3, Table S3) and 34.5% D_2O/H_2O (vol./vol.). However, the saturated D lipids become

https://doi.org/10.1021/acssuschemeng.2c06876
ACS Sustainable Chem. Eng. 2023, 11, 1598−1609

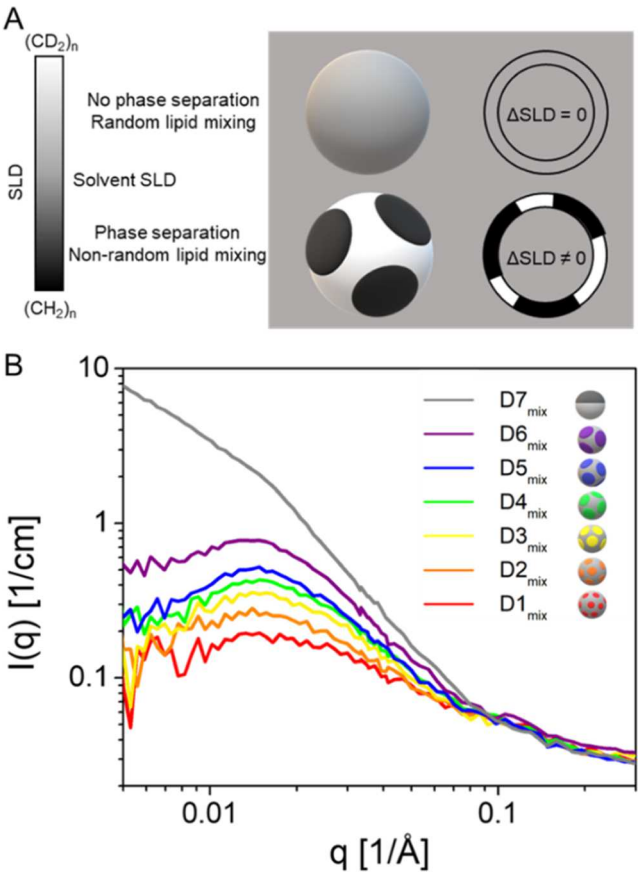

Figure 1. SANS measurements reveal phase separation through the emergence of neutron contrast with the de-mixing of deuterium-labeled saturated and unsaturated lipids. (A) Neutron contrast strategy[20] to detect phase separation is based on the emergence of local differences in SLD of a lipid mixture containing deuterated saturated acyl chains and hydrogenated saturated and unsaturated acyl chains which—on average—matches the SLD of the lipid headgroup and solvent. Upon phase separation, the non-random distribution of hydrogen and deuterium in the hydrophobic core results in local differences in the SLD and a detectable SANS signal. (B) A broad peak is observed in the mid-q range denoting the rough size of the domains.[25] This is illustrated for a family of phase-separating lipid vesicles containing POPC/DOPC/DSPC/cholesterol and exhibiting systematic variations in domain size based on hydrophobic mismatch of the co-existing phases.[25] The exact compositions are shown in Table S1.

enriched in the Lo phase upon phase separation, resulting in unequal SLD between the co-existing phases and the solvent; see Table S2. In Figure 1B, this results in a broad peak in the mid-q range of the SANS spectra, with the amplitude increasing and q-value of the peak maximum shifting to lower values with an increasing fraction of DOPC. This corresponds to larger domains and is in close agreement with earlier results and analysis from Heberle et al.[25]

Figure 2 shows the effect of adding 6% or 12% (wt/wt) EtOH (containing 34% D-EtOH to match 0.181 fm/Å^3) in the same de-mixing experiment. Figure 2A–G demonstrates a systematic increase in the size of nanodomains with increasing EtOH content. Each panel shows a different starting composition within the family of phase-separating model mixtures seen in Figure 1B. The addition of EtOH clearly shifts the broad peak associated with nanodomains to lower values of q and increases the amplitude. The increase in amplitude and shift in q parallel the effect of increasing the DOPC fraction of the low-melting lipid. In the latter case, this effect was tied to an increase in the thickness mismatch between phases.[25]

Figure 2H quantifies the observed trends through the total scattering, also known as the Porod invariant, Q^*, across sample compositions and EtOH content. We evaluate Q^* as $Q^* = \int_{0.03}^{0.005} I(q)q^2\, dq$ to capture contributions from the average square of the mean SLD contrast (matched out here), the square of radial SLD fluctuations (transverse thickness of inhomogeneous regions), and the square of lateral SLD fluctuations (domains). To retain the same SLD in the solvent as the contrast match point of the PC headgroup (as in Figure 1A), 0, 6, and 12% of EtOH/D6-EtOH mixtures were used. The total scattering increases with domain size from sample D1 to sample D7, again consistent with the observations of Heberle et al.,[25] who ascribed this phenomenon primarily to an increase in hydrophobic thickness mismatch between the phases. The addition of EtOH also increased Q^* with increasing volume fraction, suggesting a similar mechanism.

Figure 2A–G also shows a control measurement in which the temperature of the samples was increased to 70 °C, which leads to phase miscibility, homogeneously mixed lipids, and the null-scattering condition referred to above. Only composition D7 displays significant, though lessened, scattering in the null condition. This composition also showed higher scattering, even under the null condition in prior work.[25]

To illustrate the effect of EtOH on the D7 composition more clearly, we performed confocal fluorescence microscopy. The D7 composition is reported to form microscopic domains in large vesicles.[26] Confocal fluorescence microscopy is suited to micron-scale domains, with representative images shown in Figure 3. In this experiment, 0.1 mole % of the fluorescently labeled lipid, 1,2-dipalmitoyl-*sn*-glycero-3-phosphoethanolamine-*N*-(7-nitro-2-1,3-benzoxadiazol-4-yl) (NBD-DPPE), was added to the D7 composition. This dye differentially partitions between the co-existing phases, highlighting one phase. There is some ambiguity as to the phase preference of this dye in the literature, as it was previously reported to partition into the Ld phase in a different DOPC/DPPC/Chol. composition (50/27/23 mole fraction) membrane[28] but was also reported to partition into the Lo phase in giant plasma membrane vesicles.[29]Figure 3 illustrates the changes brought on by the addition of 6 and 12% (wt/wt) EtOH. Such changes in the relative curvatures of the coexisting phases are reminiscent of prior results illustrating the effect of thickness mismatch and line tension using confocal fluorescence microscopy.[21]

Hydrophobic Thickness Mismatch Increases upon Addition of EtOH. We next examine the transverse structure of the individual coexisting phases using SANS and MD simulations. Studying the structure of each coexisting phase separately allows us to assess the hydrophobic mismatch and determine how this property is altered by the presence of EtOH.

We begin with SANS measurements of the individual coexisting phases of the D1 and D7 compositions. The compositions of the constituent Ld and Lo phases are known[22−25] and can be prepared separately as vesicles. The exact compositions are listed in Table S3. The optimum SLD contrast for these measurements uses hydrogenated lipids and a deuterated solvent. This is a different contrast scheme than that described above; here, we are focused on maximizing contrast in the transverse dimension of the bilayer.

https://doi.org/10.1021/acssuschemeng.2c06876
ACS Sustainable Chem. Eng. 2023, 11, 1598−1609

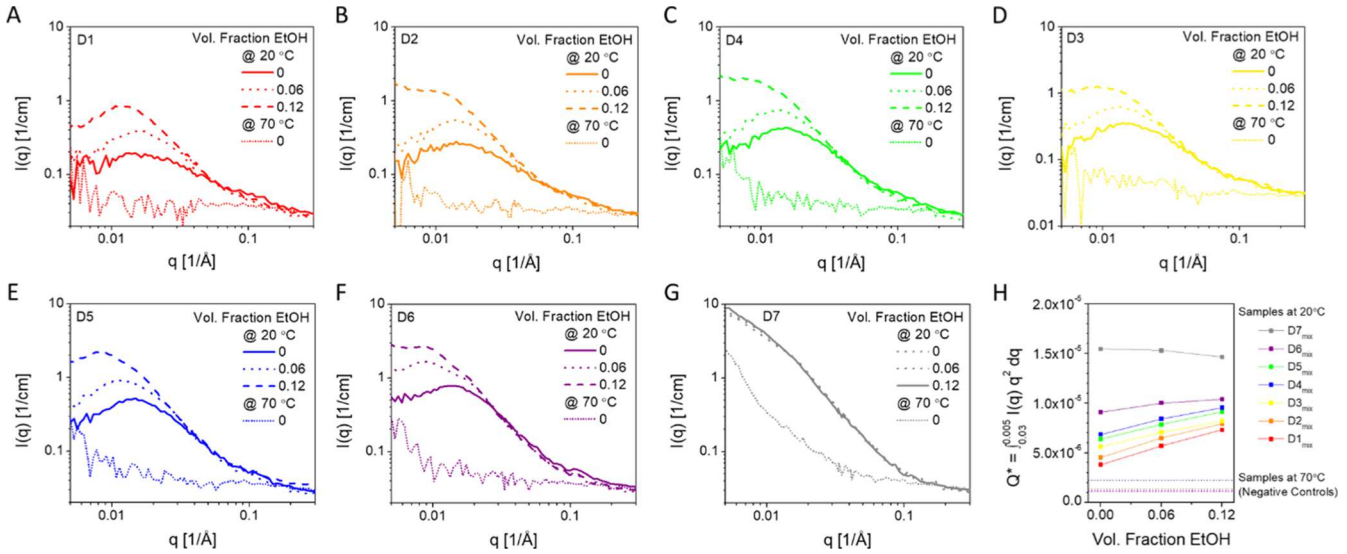

Figure 2. Effect of EtOH on nanoscopic lipid domains using contrast variation SANS. (A–G) Result of a de-mixing experiment parallel to the results shown in Figure 1. Here, 0, 0.06, or 0.12 volume fraction of D6-EtOH/EtOH (34%/66% vol./vol.) contrast-matched to the SLD of the PC headgroup was added. Upon addition of EtOH, the scattering amplitude increases and the peak center shifts to lower q. This is consistent with an increase in the size of the nanodomain. A positive control measurement is included showing the null-scattering resulting from homogeneously mixed lipids—achieved by increasing the temperature to 70 °C. (H) The Porod invariant, Q^*, represents total scattering and increases with increasing domain size, as a function of EtOH added. The D7 composition is known to form micron-scale domains and is ill-suited to this approach.

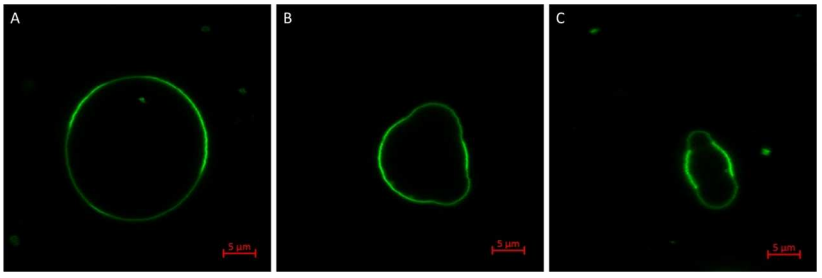

Figure 3. Confocal fluorescence microscopy shows the phase behavior of the D7 composition (DOPC/DSPC/Chol.) as giant unilamellar vesicles (GUVs) containing 0.5 mole % percent NBD-DPPE at room temperature (~20 °C). Clear morphological changes were observed upon the addition of EtOH at (A) 0%, (B) 6% (wt/wt), and (C) 12% (wt/wt).

Figure 4 summarizes the experimentally determined transverse structure of the individual phases. We used the two-parameter partition coefficient model[30] to extract the structure from the SANS data, shown in Figure S1. This model explicitly invokes molecular volumes and scattering lengths in a symmetric three-slab model, introducing the partition coefficient to account for the EtOH molecules which enter the headgroup and hydrophobic core of the bilayer.[30] Treating the data this way allows us to account for the partitioning, K_p, and localization, P_s, of the co-solvent as well as extract an explicit structural description, estimating the water content, n_w; area per lipid, APL; thickness of the hydrophobic core, $2D_C$; and thickness of the lipid head group, D_H.

We can subsequently estimate the hydrophobic thickness, t^{**}, using the formula $t^{**} = 2D_C + D_H$. The hydrophobic thickness mismatch, 2δ, is then obtained as the difference in thickness between Ld and Lo phases. We observe the mismatch increasing from 4.5 to 6.3 Å for the D1 composition and from 9.9 to 11.2 Å in the D7 composition upon the addition of EtOH at 0.06% (wt/wt). The trade-off of the two-parameter partition coefficient approach[30] is a slightly lower quality of fit when compared to a previously used asymmetric model,[25] though the hydrophobic thickness estimates obtained from either approach are similar. A comparison is included in the Supporting Information, Figure S1, and it is important to reiterate that the two-parameter partition coefficient approach[30] allowed us to extract bilayer thickness measurements that are directly linked to a physical model rather than a phenomenological estimate of thickness.

The change in the hydrophobic mismatch upon the addition of EtOH appears to come primarily from thinning of the Ld phase: 1.7 Å for the D1 composition and 1.4 Å for the D7 composition. The Lo phase, on the other hand, showed very little change in its measured thickness. As we will discuss in the next section, this is related to a greater partitioning of EtOH into the disordered phase. The EtOH content appears to compete with water in the headgroup region, partially dehydrating the headgroup of the lipids in addition to increasing the APL by its presence in the hydrophobic core in the Ld phases.

Differential Partitioning of EtOH between Coexisting Phases. MD simulations were carried out in parallel to the SANS experiments. Lipid patches of ~300 lipids matching the Ld and Lo phases for the D1 and D7 compositions were

https://doi.org/10.1021/acssuschemeng.2c06876
ACS Sustainable Chem. Eng. 2023, 11, 1598–1609

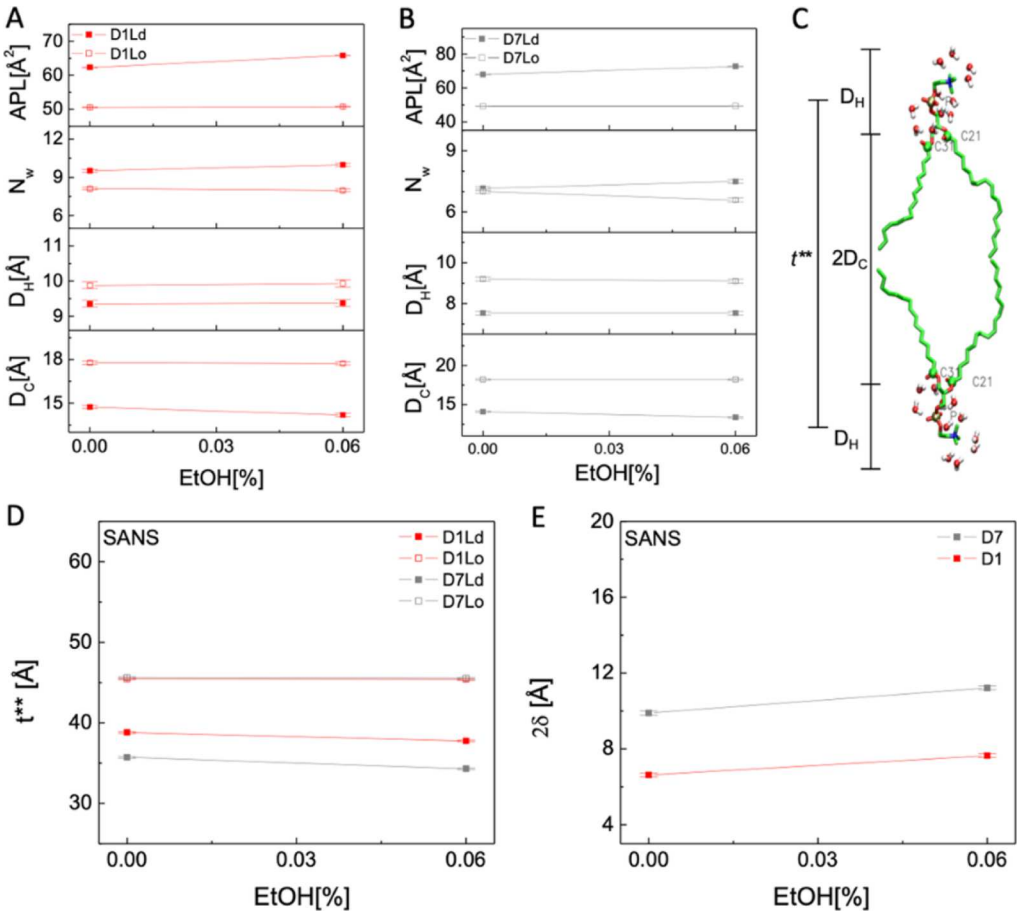

Figure 4. SANS is used to examine the transverse structure of the co-existing phases. Here, we report the structure as determined by the two-parameter partition coefficient model[30] for the individual Ld and Lo phases of the (A) D1 and (B) D7 compositions, both with and without the presence of EtOH at 6% (wt/wt). (C) We utilize this structural picture to estimate (D) the hydrophobic thickness, t^{**}, from which we can assess (E) the hydrophobic thickness mismatch, 2δ, between the phases. This analysis shows that the partitioning of EtOH leads to an increase in the hydrophobic thickness mismatch between the phases.

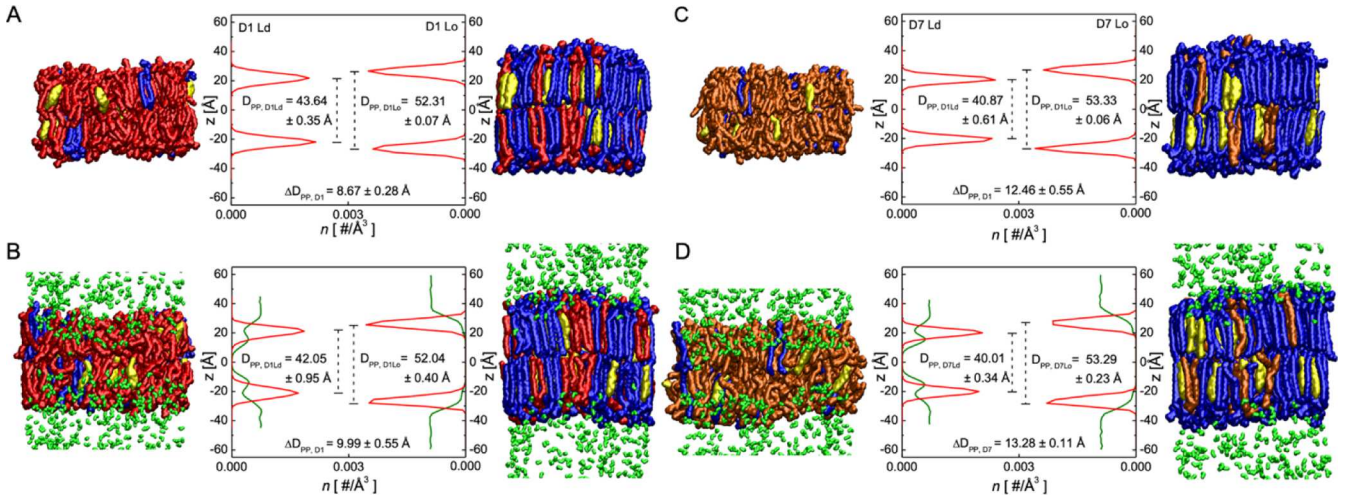

Figure 5. MD simulations were performed for (A) the D1 Ld (left) and Lo (right) phase, (B) the D1 Ld (left) and Lo (right) phase with 6% wt/wt EtOH, (C) the D7 Ld (left) and Lo (right) phase, and (D) the D7 Ld (left) and Lo (right) phase with 6% wt/wt EtOH. (POPC: red, DOPC: orange, DSPC: blue, Chol.: yellow, EtOH: green; water not shown). Each panel presents a z-profile of P number density (red line) and EtOH number density (green line). The phosphorous−phosphorous spacing, D_{PP}; the hydrophobic mismatch between Ld and Lo phases for a given composition, ΔD_{PP}; the partition coefficient, K_p; and the distribution parameter, P_s are also listed.

produced using CHARMM-GUI[31] and solvated either in water or in water with EtOH. EtOH molecules were added to achieve ∼0.06 weight fraction EtOH in the water phase of the simulation after full partitioning was achieved. We utilized the

https://doi.org/10.1021/acssuschemeng.2c06876
ACS Sustainable Chem. Eng. 2023, 11, 1598−1609

Table 1. MD-Derived Parameters[a]

sample	phase	S_{tilt}	S_{splay}	B_i [kBT]	D_{PP} [Å]	ΔD_{PP} [Å]	K_p	P_s
D1	Ld	0.842 ± 0.004	0.775 ± 0.012	22.8 ± 1.9	43.64 ± 0.35	8.67 ± 0.28		
	Lo	0.952 ± 0.005	0.945 ± 0.004	62.9 ± 2.9	52.31 ± 0.07			
D1 w/6% EtOH	Ld	0.804 ± 0.005	0.713 ± 0.009	17.0 ± 0.9	42.05 ± 0.95	9.99 ± 0.55	0.34 ± 0.01	0.45 ± 0.01
	Lo	0.943 ± 0.013	0.949 ± 0.003	67.3 ± 4.8	52.04 ± 0.40		0.11 ± 0.01	0.17 ± 0.07
D7	Ld	0.807 ± 0.010	0.690 ± 0.011	14.4 ± 1.2	48.87 ± 0.61	12.46 ± 0.55		
	Lo	0.960 ± 0.001	0.951 ± 0.002	68.0 ± 1.2	53.33 ± 0.06			
D7 w/6% EtOH	Ld	0.770 ± 0.005	0.633 ± 0.010	13.0 ± 2.9	40.01 ± 0.34	13.28 ± 0.11	0.41 ± 0.01	0.39 ± 0.01
	Lo	0.957 ± 0.002	0.948 ± 0.003	67.0 ± 2.6	53.29 ± 0.23		0.11 ± 0.01	0.13 ± 0.03

[a] S_{tilt}—tilt order parameter; S_{splay}—splay order parameter; B_i—bending modulus; D_{PP}—hydrophobic thickness assessed a phosphorous−phosphorous spacing; ΔD_{PP}—the hydrophobic mismatch between Ld and Lo for a given composition; K_p—patrician coefficient; P_s—distribution parameter

octanol−water partition coefficient to estimate this a priori. Due to the observed difference in partition coefficient for the two phases, the final concentrations varied within ±0.005 of the 0.06 weight fraction target. The full box compositions can be found in Table S5. A total of 1.2 μs of MD trajectories was obtained for each condition. This was achieved as three independent replicates of each condition, with a preliminary run of 600 ns to gauge convergence and two additional independent runs of 300 ns; see Figures S2−S4. The final 150 ns of each trajectory was used for analysis. In total, 24 simulations were performed, covering 9.6 μs of the all-atom trajectory time.

Figure 5 summarizes the result of these simulations, highlighting changes in the bilayer structure upon EtOH addition, along with the partitioning parameters. It is readily apparent that the Ld phases are thinner and less ordered and have a greater amount of co-solvent partitioning inside than that of the Lo phase bilayers for both D1 and D7 compositions. Table 1 lists the relevant parameters calculated from the simulations, including the tilt order parameter, S_{tilt}; the splay order parameter, S_{splay}; the bending modulus, B_i; the hydrophobic thickness assessed by the phosphorous−phosphorous spacing, D_{PP}; the hydrophobic mismatch between Ld and Lo phases for a given composition, ΔD_{PP}; the partition coefficient, K_p; and the distribution parameter, P_s. From the simulation, we define K_p as[32]

$$K_p = \frac{C_s^{Lipid}}{C_s^{Bulk}} = \frac{\frac{\int_0^z HG_{n_{EtOH}} dz}{\int_0^z HG\, dz}}{\frac{\int_{z_{HG}}^{z_{box}} n_{EtOH}\, dz}{\int_{z_{HG}}^{z_{box}} dz}} \quad (6)$$

where C_s^{Lipid} and C_s^{Bulk} are the concentrations of EtOH in the lipid phase and bulk solvent phase, respectively, and n_{EtOH} represents the number density of EtOH molecules in the z-profile. The number density of EtOH can be numerically integrated within defined regions of the structure to obtain the concentration (i.e., the center of the bilayer to the edge of the lipid headgroup to represent the lipid phase or from the edge of the lipid headgroup to the edge of the box). This is analogous to the way we defined the partition coefficient in the two-parameter partition constant model, which defines K_p on a per-lipid basis using molecular volumes as

$$K_p = \frac{C_s^{Lipid}}{C_s^{Bulk}} = \frac{\frac{N_s^{Lipid}}{(N_s^{Lipid}V_s + N_w^{Lipid}V_w + V_h + V_c)}}{\frac{N_s^{Bulk}}{N_s^{Bulk}V_s + N_w^{Bulk}V_w}} \quad (7)$$

Here, N_s^{Lipid} and N_s^{Bulk} represent the number of EtOH molecules in the lipid and bulk phases (on a per lipid basis), and N_w^{Lipid} and N_w^{Bulk} are the number of water molecules in the lipid and bulk phases (on a per lipid basis). V_s, V_w, V_h, and V_c are the molecular volumes for the EtOH, water, the average lipid headgroup, and the average lipid tail region.

The simulations show that the addition of EtOH has a marked thinning and disordering effect on the Ld phase of both the D1 and D7 compositions. The D1 Ld composition was thinned by 1.5 Å as defined by D_{PP}, while the D7 Ld composition was thinned by 0.85 Å. The addition of 6% (wt/wt) EtOH had a less pronounced effect on the thickness of the Lo phases, with the D1 and D7 Lo compositions thinning by 0.3 and 0 Å, respectively. The hydrophobic thickness mismatch therefore increases upon EtOH addition in the simulations, increasing by 1.3 and 0.8 Å for D1 and D7, respectively. t^{**} and D_{PP} are related, but different, definitions of hydrophobic thickness; see the Supporting Information.

The simulations and experiments show that EtOH has a greater impact on the structure of the Ld phase than that of the Lo phase. Indeed, Figure 5 shows a clear difference in the amount of EtOH entering the Ld and Lo systems, with more EtOH in the Ld phase and more of that EtOH penetrating the hydrophobic core of the bilayer. This can be defined quantitatively using a two-parameter partition coefficient approach, parallel to the analysis of the SANS data.[30] We can define an overall partition coefficient, K_p, and a distribution parameter, P_s, which specifies where EtOH is found (0 to 1 range, with 0 indicating EtOH in the headgroup region or 1 indicating all the EtOH in the hydrophobic tail region). As detailed in Figure 5 and Table 1, we calculated the partition coefficients from the MD simulations, finding values of 0.34 for D1 Ld, 0.41 for D7 Ld, 0.11 for D1 Lo, and 0.11 for D7 Lo. Our results agree with the magnitude of the octanol/water partition coefficient of EtOH, 0.49,[33,34] which is the traditional estimate of lipid partitioning used in pharmacological studies (Meyer−Overton correlation). We see that K_p is 3−4 times larger in the Ld phases than in the Lo phases. The decreased EtOH content in the cholesterol-rich Lo phases is consistent with earlier results of cholesterol content, decreasing the partitioning of EtOH.[35] Before using these values for K_p, it should be noted that there is a concentration dependence for the partition coefficient of EtOH in lipid membranes,[36] with the value of K_p dropping with the increasing concentration of EtOH. The lipid literature often reports the partition coefficient for EtOH (or other substance) as the ratio of mole fractions for EtOH in the lipid phase to the mole fraction of EtOH in the water phase.[35−37] If we were to report our

https://doi.org/10.1021/acssuschemeng.2c06876
ACS Sustainable Chem. Eng. 2023, 11, 1598−1609

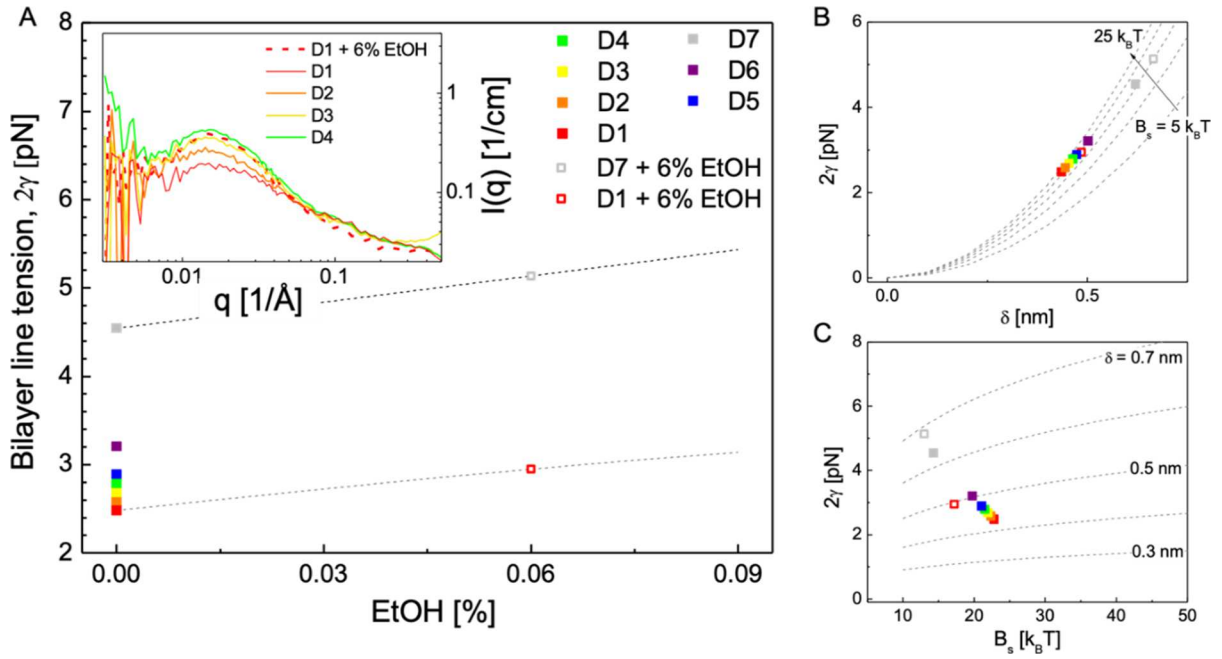

Figure 6. (A) Estimates of bilayer line tension for D1 to D7 family of lipid compositions along with the D1 and D7 compositions in the presence of 6% (wt/wt) EtOH. Inset: SANS de-mixing experiment spectra comparing the profile for the D1 composition with 6% (wt/wt) EtOH to the D3 and D4 compositions, which have similar estimated line tensions. (B) Bilayer line tension as a function of monolayer hydrophobic thickness mismatch, δ, or (C) as a function of bending modulus of the surround phase, Bs.

results using the same basis, K_p would be 12.4 for D1 Ld, 4.0 for D1 Lo, 14.6 for D7 Ld, and 3.9 for D7 Lo, in agreement with the magnitude of those results.

The location of EtOH differs between the Ld and Lo phase systems, with EtOH accumulating near the headgroup/tail interface of lipids in both Ld systems. This is consistent with experimental and MD observations of EtOH location in fluid-phase single-component phosphatidylcholine lipid membranes.[7,38] In the Lo phases, we do not see such accumulation at the interface. Our model estimates the location of EtOH using P_s, which results in values of 0.45 for D1 Ld, 0.39 for D7 Ld, 0.17 for D1 Lo, and 0.13 for D7 Lo. This quantifies the picture in Figure 5, telling us that 85−90% of the EtOH which partitions into the Lo systems is located in the headgroup region, while 55−60% of the EtOH is in the headgroup for the Ld systems.

Impact of EtOH on Membrane Packing and Mechanical Properties. The differential partitioning of the EtOH between the coexisting phases also leads to differential softening and disordering of one phase relative to the other. We can characterize these effects from our simulations through parameters such as the splay and tilt order parameters, S_{splay} and S_{tilt}, as well as the bending modulus,[39] B_i. Figure S5 provides a visual description of the underlying tilt and splay angles. The tilt angle refers to the angle between a given lipid and the bilayer normal, while a splay angle is defined as the angle between two lipids. The order parameters are defined such that a value of 1 would indicate a perfectly aligned system, such as the lipids oriented parallel to the vector normal or two lipids aligned parallel to each other. A value of 0 indicates a random orientation, and a value of −0.5 indicates antiparallel orientation.

We list S_{splay} and S_{tilt} for the D1 and D7 pure phases with and without EtOH in Table 1. As their names would indicate, the D1 and D7 Ld phases have lower order parameters than the D1 and D7 Lo phases. The addition of EtOH has a marked disordering effect on the Ld phase, reducing S_{tilt} by ∼5% and S_{splay} by ∼10%. Yet, as we might anticipate from the structural studies and Figure 5, the Lo phases are less affected by the addition of EtOH. Both S_{splay} and S_{tilt} are relatively unchanged, staying within 1% of the original values.

The bending modulus, B_i, can be computed[39] from the tilt and splay angles obtained from the MD trajectories. The addition of EtOH causes a decrease in the bending moduli for both the D1 and D7 Ld phases, with bending moduli dropping from 22.8 to 17.2 k_BT for D1 Ld and from 14.4 to 13.0 k_BT for D7 Ld. The bending modulus of the D1 Lo systems increased upon the addition of EtOH from 62.9 to 67.3 k_BT, while the bending modulus of the D7 Lo phase dropped from 68.0 to 67.0 k_BT upon the addition of EtOH. Consistent with prior observations, we observe that the Ld phase has a lower value of B_i than that of the Lo phase for the D1 composition.[24] The addition of EtOH softens the Ld phase in both compositions, while EtOH has a minimal effect on the D7 Lo phase and a slight stiffening effect on the D1 Lo phase. Returning to eq 5, we know that the line tension is influenced by the B_i of the two phases. This is exemplified by results showing how EtOH influences the mechanical properties of lipid membranes and influences phase diagrams in cholesterol (and ergosterol) -containing membranes.[40]

EtOH Effects Lead to Increased Line Tension. Having described the effect of EtOH on lipid phase behavior as well as the structure and mechanical properties of the co-existing phases, we can begin to contextualize these observations in terms of the bilayer line tension, 2γ. For phase-separating systems with co-existing liquid phases, 2γ is expected to be a small, positive value based on an analysis of the GUV shape,[21,41] pipette aspiration,[42] and other methods.[43] Returning to eq 5, we can estimate the line tension from our results, relying on several assumptions. The first term of eq 5

https://doi.org/10.1021/acssuschemeng.2c06876
ACS Sustainable Chem. Eng. 2023, 11, 1598−1609

represents the elastic contribution to line tension from thickness mismatch, while the second term is related to the mismatch in spontaneous curvatures and bending moduli between the phases. We will evaluate only the first term, focusing on the role of hydrophobic thickness mismatch since we would expect EtOH to influence the spontaneous curvature of both phases but particularly the EtOH-rich Ld phase. It might also be anticipated that EtOH partitioning will strongly reduce the spontaneous curvature of the Ld phase in these systems. Curvature changes may turn out to be a significant effect, especially when evaluating the second term. Without a reasonable estimate of the spontaneous curvature change, we cannot accurately evaluate the second term of eq 5. Because of this, we will neglect the second term and use the following expression to estimate the elastic bilayer line tension, 2γ

$$2\gamma \sim \frac{2\sqrt{B_S K_S B_D K_D}}{\sqrt{B_D K_D} + \sqrt{B_S K_S}} \frac{\delta^2}{{h_0}^2} \quad (8)$$

We have used the results of the MD simulations as the input parameters for B_i, δ, and h_0. K_i is assumed as 10 k_BT/nm^2 for all systems,[44] consistent with prior investigations.[20]

Figure 6 shows the calculated bilayer line tensions for the D1 to D7 family of phase-separating lipid compositions. Upon the addition of EtOH, 2γ is seen to increase from 2.5 to 2.9 pN for the D1 composition and from 4.5 to 5.1 pN for the D7 composition. In Figure 6A, we also provide an estimate for the bilayer line tension for the full family of compositions from D1 to D7 at 0% EtOH. This is obtained using a linear interpolation of the simulation-derived parameters, B_S, B_D, δ, and h_0, obtained for D1 and D7 as inputs for D2 to D6. The linear interpolation is based on the linear trend in hydrophobic mismatch and the ρ parameter defined by Heberle et al.,[25] which represents the fraction of DOPC over the total low-melting lipid content. We then evaluated eq 8 to obtain 2γ. A continuous estimate of 2γ as a function of EtOH content shown for D1 and D7 (the dotted lines on Figure 6A) was similarly obtained, assuming a linear dependence of B_S, B_D, δ, and h_0 between our results obtained for D1 and D7 with and without 6% (wt/wt) EtOH.

Each of these analyses shows the clear trend of increasing bilayer line tension with increasing hydrophobic thickness mismatch. This was true whether the increase in thickness mismatch originated from compositional changes (DOPC content) or the addition of EtOH. Indeed, the effect of EtOH on the line tension and the hydrophobic thickness mismatch appears to be quite similar to a change in the lipid content from POPC to DOPC (Figure 6B). Looking back to the size of the nanodomains as measured in the SANS de-mixing experiments, the inset shows the close comparison of the D1 composition in the presence of 6% EtOH to the EtOH-free D3 and D4 mixtures. Together, we show that domain size correlates to the line tension which, in turn, correlates to the thickness mismatch.

This result should be understood with several caveats. Beyond the EtOH-induced changes in thickness mismatch, we find small changes in the bending modulus when ethanol is present, with ordered phases becoming slightly more stiff and disordered phases becoming more flexible. The reported values of 2γ should be understood as high estimates of the true value, as the full form of eq 5 would decrease the quantity 2γ for the nonzero spontaneous curvature of either phase. Indeed, EtOH will likely also alter the spontaneous curvature, and it would also be reasonable to expect solvent-induced changes in the composition of the co-existing phases as ethanol complicates the phase equilibria. Indeed, compensatory compositional changes between the individual phases might be expected.[45] Nevertheless, the analysis shows an increase in line tension, a result which favors larger domains and provides an explanation for our observations of nanodomain size increase upon the EtOH addition seen in Figures 2 and 3.

Biological Context. We have demonstrated co-solvent-induced changes in model phase-separating lipid compositions and established a physical basis for these observations. This brings the discussion back to the biological relevance of domains and the potential impact of co-solvent-induced domain disruption. Our work here should not be taken to imply that other effects are also not important in the context of co-solvent-induced cell stress. Allosteric, metabolic, and overall membrane disruptions are also important factors. Here, allosteric effects refer to the non-specific binding of co-solvents to cellular proteins, altering their structure and function.[46,47] Metabolic effects refer to a broad set of changes in cellular metabolism,[48] proteome,[49,50] and lipidome[51−53] induced due to evolved stress responses to solvent exposure. These responses are typically regulated by stress response factors evolved to survive environmental changes such as heat, cold, salt, or ethanol.[53−55] Notably, ethanol stress responses are typically similar to heat shock responses—which would also fluidize the cell membrane.

Domains are a known feature of microbial cell membranes.[16,56] Yet the identity of membrane domain-associated proteins and their specific functions in the context of solvent stress is a topic which is yet to be investigated fully. Flotillin (FloA and FloT) and histidine kinase (KinC) are one possible set of early candidates identified in the literature studies.[11,16] The kinase activity, phosphorylating the sporulation factor Spo0A,[17] is lost with domain disruption. Spo0A is a global regulator which controls sporulation, cell growth, and metabolism (acidogenesis and solventogenesis). Indeed, recent work has shown strong evidence of the effect of Spo0A on solvent tolerance in *C. acetobytylicum*.[18] A single knockout was able to abort sporulation at the initiation stage, which enhanced butanol tolerance and production. The importance of FMMs is not limited to sporulation.[11] Recent studies have shown that the disruption of microdomains leads to other deficits in microbial cell function. The case of methicillin resistance in the pathogen methicillin-resistant *Staphylococcus aureus* (MRSA) is a well-known example.[15] Here, a disruption of membrane domains led to a loss of methicillin resistance due to the decrease in efficiency of PBP2a oligomerization within the membrane domains. Disruption of membrane domains was also reported to impact protein secretion and biofilm formation.[11,12]

CONCLUSIONS

We have demonstrated that EtOH drives a coarsening of lipid domains in model membranes and provided a mechanism by which EtOH increases hydrophobic mismatch between the co-existing phases, leading to an increase in the domain line tension, a driver to minimize the domain interface to domain area ratio. This represents the physical basis for a novel mode of co-solvent-induced cell stress due to FMM disruption, at concentrations below those required for destabilization of the transverse membrane structure—and loss of membrane potential.

https://doi.org/10.1021/acssuschemeng.2c06876
ACS Sustainable Chem. Eng. 2023, 11, 1598−1609

Using SANS, we have performed de-mixing studies which illustrate a coarsening of membrane domains in the presence of ethanol. Confocal fluorescence microscopy further demonstrates the effect of EtOH on micron-scale domains. We then performed additional measurements and simulations on the individual co-existing phases to understand the relative partitioning of EtOH and extract the detailed structural and mechanical descriptions. These parameters are what allow us to estimate the magnitude of the increase in line tension. Analysis then reveals that all other things held equal, an increased line tension would favor a decrease in the ratio of interfacial length to area.

Once validated by further study, this hypothesis will lead to a more holistic understanding of co-solvent stress and guide new approaches to mitigate it. Co-solvent-tolerant strain development frequently targets fatty acid or sterol compositions, efflux pumps, the introduction or modification of enzymes for in situ detoxification, or the manipulation of other evolved stress responses.[57−59] Approaches, such as ion supplementation and efflux pump modifications,[60,61] may need to be considered in a new light of membrane phase behavior.[62,63] Applications in healthcare might also be envisioned, such as the long-established link between alcohol consumption and gastrointestinal/esophageal cancers.[64] Regardless of the cell type or the specific community of researchers; our results suggest that targeting the dissociation or dispersal of domain-associated proteins, protein oligomers, or complexes may be a productive strategy to ameliorate the effects of co-solvent stress.

■ ASSOCIATED CONTENT

Supporting Information

The Supporting Information is available free of charge at https://pubs.acs.org/doi/10.1021/acssuschemeng.2c06876.

D1 to D7 sample compositions, compositions of individual co-existing phases upon phase separation, compositions and scattering length density of D1 and D7 pure phase samples at 20°C, neutron-bound coherent scattering length, molecular volume, and coherent scattering length densities of related components at 60°C, MD simulation composition, SANS data and fitting, time course of the MD box area for D1 and D7 pure phase compositions, comparison of the time course of the MD box area for the 600 ns run of all samples, and graphical representation of the splay angle and tilt angle used in analysis of the MD simulation trajectories (PDF)[65−87]

■ AUTHOR INFORMATION

Corresponding Author

Jonathan D. Nickels − *Department of Chemical and Environmental Engineering, University of Cincinnati, Cincinnati, Ohio 45220, United States;* orcid.org/0000-0001-8351-7846; Email: Jonathan.nickels@uc.edu

Authors

Luoxi Tan − *Department of Chemical and Environmental Engineering, University of Cincinnati, Cincinnati, Ohio 45220, United States*

Haden L. Scott − *Neutron Scattering Division, Oak Ridge National Laboratory, Oak Ridge, Tennessee 37830, United States;* orcid.org/0000-0002-5778-4905

Micholas Dean Smith − *Department of Biochemistry and Cellular and Molecular Biology, University of Tennessee, Knoxville, Tennessee 37996, United States; Center for Molecular Biophysics, University of Tennessee/Oak Ridge National Laboratory, Oak Ridge National Laboratory, Oak Ridge, Tennessee 37831, United States;* orcid.org/0000-0002-0777-7539

Sai Venkatesh Pingali − *Neutron Scattering Division, Oak Ridge National Laboratory, Oak Ridge, Tennessee 37830, United States;* orcid.org/0000-0001-7961-4176

Hugh M. O'Neill − *Neutron Scattering Division, Oak Ridge National Laboratory, Oak Ridge, Tennessee 37830, United States;* orcid.org/0000-0003-2966-5527

Jennifer L. Morrell-Falvey − *Biosciences Division, Oak Ridge National Laboratory, Oak Ridge, Tennessee 37830, United States;* orcid.org/0000-0002-9362-7528

John Katsaras − *Neutron Scattering Division, Oak Ridge National Laboratory, Oak Ridge, Tennessee 37830, United States; Shull Wollan Center, Oak Ridge National Laboratory, Oak Ridge, Tennessee 37831, United States;* orcid.org/0000-0002-8937-4177

Jeremy C. Smith − *Department of Biochemistry and Cellular and Molecular Biology, University of Tennessee, Knoxville, Tennessee 37996, United States; Center for Molecular Biophysics, University of Tennessee/Oak Ridge National Laboratory, Oak Ridge National Laboratory, Oak Ridge, Tennessee 37831, United States;* orcid.org/0000-0002-2978-3227

Brian H. Davison − *Biosciences Division, Oak Ridge National Laboratory, Oak Ridge, Tennessee 37830, United States*

James G. Elkins − *Biosciences Division, Oak Ridge National Laboratory, Oak Ridge, Tennessee 37830, United States*

Complete contact information is available at: https://pubs.acs.org/10.1021/acssuschemeng.2c06876

Author Contributions

L.T., H.L.S., M.D.S., S.V.P., H.M.O., J.K., J.C.S., B.H.D., J.G.E., and J.D.N. conceived and designed the project. L.T., H.L.S., S.V.P., J.L.M-F., and J.D.N. performed and analyzed experiments. L.T. and M.D.S. performed and analyzed MD simulations. J.D.N. and L.T. prepared the initial manuscripts. All authors edited and approved the manuscript.

Notes

The authors declare no competing financial interest.

■ ACKNOWLEDGMENTS

This research was supported by the Genomic Science Program, Office of Biological and Environmental Research, U.S. Department of Energy (DOE), under Contract FWP ERKP752. This material is based on the work supported by the National Science Foundation under grant no. 2146264. A portion of this research used resources at the High Flux Isotope Reactor and Spallation Neutron Source, a DOE Office of Science User Facility operated by the Oak Ridge National Laboratory.

■ REFERENCES

(1) Stanley, D.; Bandara, A.; Fraser, S.; Chambers, P. J.; Stanley, G. A. The ethanol stress response and ethanol tolerance of Saccharomyces cerevisiae. *J. Appl. Microbiol.* **2010**, *109*, 13−24.

(2) Liu, S.; Qureshi, N. How microbes tolerate ethanol and butanol. *New Biotechnol.* **2009**, *26*, 117−121.

(3) Ingram, L. O. N.; Buttke, T. M.Effects of Alcohols on Micro-Organisms. In *Advances in Microbial Physiology*; Rose, A. H., Tempest, D. W., Eds.; Academic Press, 1985; Vol. *25*; pp 253−300.
(4) Ingólfsson, H. I.; Andersen, O. S. Alcohol's Effects on Lipid Bilayer Properties. *Biophys. J.* **2011**, *101*, 847−855.
(5) Ding, J.; Huang, X.; Zhang, L.; Zhao, N.; Yang, D.; Zhang, K. Tolerance and stress response to ethanol in the yeast Saccharomyces cerevisiae. *Appl. Microbiol. Biotechnol.* **2009**, *85*, 253−263.
(6) Chin, J. H.; Goldstein, D. B. Drug Tolerance in Biomembranes: A Spin Label Study of the Effects of Ethanol. *Science* **1977**, *196*, 684−685.
(7) Patra, M.; Salonen, E.; Terama, E.; Vattulainen, I.; Faller, R.; Lee, B. W.; Holopainen, J.; Karttunen, M. Under the Influence of Alcohol: The Effect of Ethanol and Methanol on Lipid Bilayers. *Biophys. J.* **2006**, *90*, 1121−1135.
(8) Leão, C.; Van Uden, N. Effects of ethanol and other alkanols on passive proton influx in the yeast Saccharomyces cerevisiae. *Biochim. Biophys. Acta, Biomembr.* **1984**, *774*, 43−48.
(9) Cartwright, C. P.; juroszek, J.-R.; Beavan, M. J.; Ruby, F. M. S.; De Morais, S. M. F.; Rose, A. H. Ethanol Dissipates the Proton-motive Force across the Plasma Membrane of Saccharomyces cerevisiae. *Microbiology* **1986**, *132*, 369−377.
(10) Cartwright, C. P.; Verzey, F. J.; Rose, A. H. Effect of Ethanol on Activity of the Plasma-membrane ATPase in, and Accumulation of Glycine by, Saccharomyces Cerevisiae. *Microbiology* **1987**, *133*, 857−865.
(11) Lopez, D.; Koch, G. Exploring functional membrane microdomains in bacteria: an overview. *Curr. Opin. Microbiol.* **2017**, *36*, 76−84.
(12) López, D.; Kolter, R. Functional microdomains in bacterial membranes. *Genes Dev.* **2010**, *24*, 1893−1902.
(13) London, E.; Brown, D. A. Insolubility of lipids in triton X-100: physical origin and relationship to sphingolipid/cholesterol membrane domains (rafts). *Biochim. Biophys. Acta, Biomembr.* **2000**, *1508*, 182−195.
(14) Schuck, S.; Simons, K. Polarized sorting in epithelial cells: raft clustering and the biogenesis of the apical membrane. *J. Cell Sci.* **2004**, *117*, 5955−5964.
(15) García-Fernández, E.; Koch, G.; Wagner, R. M.; Fekete, A.; Stengel, S. T.; Schneider, J.; Mielich-Süss, B.; Geibel, S.; Markert, S. M.; Stigloher, C.; Lopez, D. Membrane Microdomain Disassembly Inhibits MRSA Antibiotic Resistance. *Cell* **2017**, *171*, 1354−1367.
(16) López, D.; Kolter, R. Functional microdomains in bacterial membranes. *Genes Dev.* **2010**, *24*, 1893−1902.
(17) LeDeaux, J. R.; Grossman, A. D. Isolation and characterization of kinC, a gene that encodes a sensor kinase homologous to the sporulation sensor kinases KinA and KinB in Bacillus subtilis. *J. Bacteriol.* **1995**, *177*, 166−175.
(18) Du, G.; Zhu, C.; Xu, M.; Wang, L.; Yang, S.-T.; Xue, C. Energy-efficient butanol production by Clostridium acetobutylicum with histidine kinase knockouts to improve strain tolerance and process robustness. *Green Chem.* **2021**, *23*, 2155−2168.
(19) Helfrich, W. Elastic Properties of Lipid Bilayers: Theory and Possible Experiments. *Z. Naturforsch., C* **1973**, *28*, 693−703.
(20) Kuzmin, P. I.; Akimov, S. A.; Chizmadzhev, Y. A.; Zimmerberg, J.; Cohen, F. S. Line tension and interaction energies of membrane rafts calculated from lipid splay and tilt. *Biophys. J.* **2005**, *88*, 1120−1133.
(21) García-Sáez, A. J.; Chiantia, S.; Schwille, P. J. J. o. B. C. Effect of line tension on the lateral organization of lipid membranes. *J. Biol. Chem.* **2007**, *282*, 33537−33544.
(22) Feigenson, G. W. Phase diagrams and lipid domains in multicomponent lipid bilayer mixtures. *Biochim. Biophys. Acta, Biomembr.* **2009**, *1788*, 47−52.
(23) Goh, S. L.; Amazon, J. J.; Feigenson, G. W. Toward a better raft model: modulated phases in the four-component bilayer, DSPC/DOPC/POPC/CHOL. *Biophys. J.* **2013**, *104*, 853−862.
(24) Nickels, J. D.; Cheng, X.; Mostofian, B.; Stanley, C.; Lindner, B.; Heberle, F. A.; Perticaroli, S.; Feygenson, M.; Egami, T.; Standaert, R. F.; Smith, J. C.; Myles, D. A. A.; Ohl, M.; Katsaras, J. Mechanical properties of nanoscopic lipid domains. *J. Am. Chem. Soc.* **2015**, *137*, 15772−15780.
(25) Heberle, F. A.; Petruzielo, R. S.; Pan, J.; Drazba, P.; Kučerka, N.; Standaert, R. F.; Feigenson, G. W.; Katsaras, J. Bilayer thickness mismatch controls domain size in model membranes. *J. Am. Chem. Soc.* **2013**, *135*, 6853−6859.
(26) Konyakhina, T. M.; Wu, J.; Mastroianni, J. D.; Heberle, F. A.; Feigenson, G. W. Phase diagram of a 4-component lipid mixture: DSPC/DOPC/POPC/chol. *Biochim. Biophys. Acta, Biomembr.* **2013**, *1828*, 2204−2214.
(27) Jacrot, B. The study of biological structures by neutron scattering from solution. *Rep. Prog. Phys.* **1976**, *39*, 911.
(28) Baumgart, T.; Hunt, G.; Farkas, E. R.; Webb, W. W.; Feigenson, G. W. Fluorescence probe partitioning between Lo/Ld phases in lipid membranes. *Biochim. Biophys. Acta, Biomembr.* **2007**, *1768*, 2182−2194.
(29) Sengupta, P.; Hammond, A.; Holowka, D.; Baird, B. Structural determinants for partitioning of lipids and proteins between coexisting fluid phases in giant plasma membrane vesicles. *Biochim. Biophys. Acta, Biomembr.* **2008**, *1778*, 20−32.
(30) Tan, L.; Smith, M. D.; Scott, H. L.; Yahya, A.; Elkins, J. G.; Katsaras, J.; O'Neill, H. M.; Pingali, S. V.; Smith, J. C.; Davison, B. H.; et al. Modeling the partitioning of amphiphilic molecules and co-solvents in biomembranes. *J. Appl. Crystallogr.* **2022**, *55*, 1401.
(31) Jo, S.; Kim, T.; Iyer, V. G.; Im, W. CHARMM-GUI: a web-based graphical user interface for CHARMM. *J. Comput. Chem.* **2008**, *29*, 1859−1865.
(32) Katz, Y.; Diamond, J. M. Thermodynamic constants for nonelectrolyte partition between dimyristoyl lecithin and water. *J. Membr. Biol.* **1974**, *17*, 101−120.
(33) Mackay, D.; Shiu, W.-Y.; Shiu, W.-Y.; Lee, S. C.*Handbook of Physical-Chemical Properties and Environmental Fate for Organic Chemicals*, 2nd ed.; CRC Press, 2006; pp 2480−2485.
(34) Hansch, C.; Hoekman, D.; Leo, A.; Zhang, L.; Li, P. The expanding role of quantitative structure-activity relationships (QSAR) in toxicology. *Toxicol. Lett.* **1995**, *79*, 45−53.
(35) Trandum, C.; Westh, P.; Jørgensen, K.; Mouritsen, O. G. Association of ethanol with lipid membranes containing cholesterol, sphingomyelin and ganglioside: a titration calorimetry study. *Biochim. Biophys. Acta, Biomembr.* **1999**, *1420*, 179−188.
(36) Terama, E.; Ollila, O. H. S.; Salonen, E.; Rowat, A. C.; Trandum, C.; Westh, P.; Patra, M.; Karttunen, M.; Vattulainen, I. Influence of Ethanol on Lipid Membranes: From Lateral Pressure Profiles to Dynamics and Partitioning. *J. Phys. Chem. B* **2008**, *112*, 4131−4139.
(37) Nizza, D. T.; Gawrisch, K. A layer model of ethanol partitioning into lipid membranes. *Gen. Physiol. Biophys.* **2009**, *28*, 140.
(38) Holte, L. L.; Gawrisch, K. Determining Ethanol Distribution in Phospholipid Multilayers with MAS−NOESY Spectra. *Biochemistry* **1997**, *36*, 4669−4674.
(39) Khelashvili, G.; Kollmitzer, B.; Heftberger, P.; Pabst, G.; Harries, D. Calculating the bending modulus for multicomponent lipid membranes in different thermodynamic phases. *J. Chem. Theory Comput.* **2013**, *9*, 3866−3871.
(40) Tierney, K. J.; Block, D. E.; Longo, M. L. Elasticity and phase behavior of DPPC membrane modulated by cholesterol, ergosterol, and ethanol. *Biophys. J.* **2005**, *89*, 2481−2493.
(41) Baumgart, T.; Hess, S. T.; Webb, W. W. Imaging coexisting fluid domains in biomembrane models coupling curvature and line tension. *Nature* **2003**, *425*, 821−824.
(42) Tian, A.; Johnson, C.; Wang, W.; Baumgart, T. Line Tension at Fluid Membrane Domain Boundaries Measured by Micropipette Aspiration. *Phys. Rev. Lett.* **2007**, *98*, 208102.
(43) Stottrup, B. L.; TigreLazo, J.; Bagonza, V. B.; Kunz, J. C.; Zasadzinski, J. A. Comparison of Line Tension Measurement Methods for Lipid Monolayers at Liquid−Liquid Coexistence. *Langmuir* **2019**, *35*, 16053−16061.

https://doi.org/10.1021/acssuschemeng.2c06876
ACS Sustainable Chem. Eng. 2023, 11, 1598−1609

(44) May, S.; Kozlovsky, Y.; Ben-Shaul, A.; Kozlov, M. M. Tilt modulus of a lipid monolayer. *Eur. Phys. J. E* **2004**, *14*, 299−308.
(45) Nickels, J. D.; Smith, M. D.; Alsop, R. J.; Himbert, S.; Yahya, A.; Cordner, D.; Zolnierczuk, P.; Stanley, C. B.; Katsaras, J.; Cheng, X.; et al. Lipid Rafts: Buffers of Cell Membrane Physical Properties. *J. Phys. Chem. B* **2019**, *123*, 2050−2056.
(46) Iwata, S.; Ohta, T. Molecular Basis of Allosteric Activation of Bacterial l-Lactate Dehydrogenase. *J. Mol. Biol.* **1993**, *230*, 21−27.
(47) Hallsworth, J. E.; Nomura, Y.; Iwahara, M. Ethanol-induced water stress and fungal growth. *J. Ferment. Bioeng.* **1998**, *86*, 451−456.
(48) Lucero, P.; Peñalver, E.; Moreno, E.; Lagunas, R. Internal Trehalose Protects Endocytosis from Inhibition by Ethanol in Saccharomyces cerevisiae. *Appl. Environ. Microbiol.* **2000**, *66*, 4456−4461.
(49) Williams, T. I.; Combs, J. C.; Lynn, B. C.; Strobel, H. J. Proteomic profile changes in membranes of ethanol-tolerant Clostridium thermocellum. *Appl. Microbiol. Biotechnol.* **2007**, *74*, 422−432.
(50) Alexandre, H.; Rousseaux, I.; Charpentier, C. Ethanol adaptation mechanisms in Saccharomyces cerevisiae. *Biotechnol. Appl. Biochem.* **1994**, *20*, 173−183.
(51) Mishra, P.; Prasad, R. Relationship between ethanol tolerance and fatty acyl composition of Saccharomyces cerevisiae. *Appl. Microbiol. Biotechnol.* **1989**, *30*, 294−298.
(52) Šajbidor, J.; Ciesarová, Z.; Šmogrovičová, D. Influence of ethanol on the lipid content and fatty acid composition ofSaccharomyces cerevisiœ. *Folia Microbiol.* **1995**, *40*, 508−510.
(53) Hecker, M.; Völker, U. Non-specific, general and multiple stress resistance of growth-restricted Bacillus subtilis cells by the expression of the σB regulon. *Mol. Microbiol.* **1998**, *29*, 1129−1136.
(54) Hecker, M.; Schumann, W.; Völker, U. Heat-shock and general stress response in Bacillus subtilis. *Mol. Microbiol.* **1996**, *19*, 417−428.
(55) Piper, P. W. The heat shock and ethanol stress responses of yeast exhibit extensive similarity and functional overlap. *FEMS Microbiol. Lett.* **1995**, *134*, 121−127.
(56) Nickels, J. D.; Chatterjee, S.; Stanley, C. B.; Qian, S.; Cheng, X.; Myles, D. A. A.; Standaert, R. F.; Elkins, J. G.; Katsaras, J. The in vivo structure of biological membranes and evidence for lipid domains. *PLoS Biol.* **2017**, *15*, No. e2002214.
(57) Wang, S.; Sun, X.; Yuan, Q. Strategies for enhancing microbial tolerance to inhibitors for biofuel production: A review. *Bioresour. Technol.* **2018**, *258*, 302−309.
(58) Cheng, C.; Kao, K. C. How to survive being hot and inebriated. *Science* **2014**, *346*, 35−36.
(59) Lam, F. H.; Ghaderi, A.; Fink, G. R.; Stephanopoulos, G. Engineering alcohol tolerance in yeast. *Science* **2014**, *346*, 71−75.
(60) Zhao, X. Q.; Xue, C.; Ge, X. M.; Yuan, W. J.; Wang, J. Y.; Bai, F. W. Impact of zinc supplementation on the improvement of ethanol tolerance and yield of self-flocculating yeast in continuous ethanol fermentation. *J. Biotechnol.* **2009**, *139*, 55−60.
(61) Madeira, A.; Leitão, L.; Soveral, G.; Dias, P.; Prista, C.; Moura, T.; Loureiro-Dias, M. C. Effect of ethanol on fluxes of water and protons across the plasma membrane of Saccharomyces cerevisiae. *FEMS Yeast Res.* **2010**, *10*, 252−258.
(62) Poyton, M. F.; Pullanchery, S.; Sun, S.; Yang, T.; Cremer, P. S. Zn2+ binds to phosphatidylserine and induces membrane blebbing. *J. Am. Chem. Soc.* **2020**, *142*, 18679−18686.
(63) Poyton, M. F.; Sendecki, A. M.; Cong, X.; Cremer, P. S. Cu2+ binds to phosphatidylethanolamine and increases oxidation in lipid membranes. *J. Am. Chem. Soc.* **2016**, *138*, 1584−1590.
(64) Liu, Y.; Chen, H.; Sun, Z.; Chen, X. Molecular mechanisms of ethanol-associated oro-esophageal squamous cell carcinoma. *Cancer Lett.* **2015**, *361*, 164−173.
(65) Lynn, G. W.; Heller, W.; Urban, V.; Wignall, G.; Weiss, K.; Myles, D. A. Bio-SANS—a dedicated facility for neutron structural biology at Oak Ridge National Laboratory. *Phys. B* **2006**, *385*−*386*, 880−882.
(66) Arnold, O.; Bilheux, J.-C.; Borreguero, J.; Buts, A.; Campbell, S. I.; Chapon, L.; Doucet, M.; Draper, N.; Ferraz Leal, R. F.; Gigg, M.; Lynch, V. E.; Markvardsen, A.; Mikkelson, D. J.; Mikkelson, R. L.; Miller, R.; Palmen, K.; Parker, P.; Passos, G.; Perring, T. G.; Peterson, P. F.; Ren, S.; Reuter, M. A.; Savici, A. T.; Taylor, J. W.; Taylor, R. J.; Tolchenov, R.; Zhou, W.; Zikovsky, J. Mantid—Data analysis and visualization package for neutron scattering and μ SR experiments. *Nucl. Instrum. Methods Phys. Res., Sect. A* **2014**, *764*, 156−166.
(67) Doucet, M.; King, S.; Butler, P.; Kienzle, P.; Parker, P.; Krzywon, J.; Jackson, A.; Richter, T.; Gonzales, M.; Nielsen, T.*SasView*, Version 5.0. 0. Zenodo, 2019, 10.
(68) Tan, L.; Elkins, J. G.; Davison, B. H.; Kelley, E. G.; Nickels, J. Implementation of a self-consistent slab model of bilayer structure in the SasView suite. *J. Appl. Crystallogr.* **2021**, *54*, 363−370.
(69) Tristram-Nagle, S.; Liu, Y.; Legleiter, J.; Nagle, J. F. Structure of gel phase DMPC determined by X-ray diffraction. *Biophys. J.* **2002**, *83*, 3324−3335.
(70) Kučerka, N.; Nieh, M.-P.; Katsaras, J. Fluid phase lipid areas and bilayer thicknesses of commonly used phosphatidylcholines as a function of temperature. *Biochim. Biophys. Acta, Biomembr.* **2011**, *1808*, 2761−2771.
(71) Tristram-Nagle, S.; Petrache, H. I.; Nagle, J. F. Structure and interactions of fully hydrated dioleoylphosphatidylcholine bilayers. *Biophys. J.* **1998**, *75*, 917−925.
(72) Vrugt, J. A.; Ter Braak, C. J. DREAM (D): an adaptive Markov Chain Monte Carlo simulation algorithm to solve discrete, non-continuous, and combinatorial posterior parameter estimation problems. *Hydrol. Earth Syst. Sci.* **2011**, *15*, 3701−3713.
(73) Abraham, M. J.; Murtola, T.; Schulz, R.; Páll, S.; Smith, J. C.; Hess, B.; Lindahl, E. GROMACS: High performance molecular simulations through multi-level parallelism from laptops to supercomputers. *SoftwareX* **2015**, *1*−*2*, 19−25.
(74) Brooks, B. R.; Brooks, C. L., III; Mackerell, A. D., Jr; Nilsson, L.; Petrella, R. J.; Roux, B.; Won, Y.; Archontis, G.; Bartels, C.; Boresch, S.; Caflisch, A.; Caves, L.; Cui, Q.; Dinner, A. R.; Feig, M.; Fischer, S.; Gao, J.; Hodoscek, M.; Im, W.; Kuczera, K.; Lazaridis, T.; Ma, J.; Ovchinnikov, V.; Paci, E.; Pastor, R. W.; Post, C. B.; Pu, J. Z.; Schaefer, M.; Tidor, B.; Venable, R. M.; Woodcock, H. L.; Wu, X.; Yang, W.; York, D. M.; Karplus, M. CHARMM: the biomolecular simulation program. *J. Comput. Chem.* **2009**, *30*, 1545−1614.
(75) Lee, S.; Tran, A.; Allsopp, M.; Lim, J. B.; Hénin, J.; Klauda, J. B. CHARMM36 united atom chain model for lipids and surfactants. *J. Phys. Chem. B* **2014**, *118*, 547−556.
(76) Lee, J.; Cheng, X.; Swails, J. M.; Yeom, M. S.; Eastman, P. K.; Lemkul, J. A.; Wei, S.; Buckner, J.; Jeong, J. C.; Qi, Y.; Jo, S.; Pande, V. S.; Case, D. A.; Brooks, C. L.; MacKerell, A. D.; Klauda, J. B.; Im, W. CHARMM-GUI input generator for NAMD, GROMACS, AMBER, OpenMM, and CHARMM/OpenMM simulations using the CHARMM36 additive force field. *J. Chem. Theory Comput.* **2016**, *12*, 405−413.
(77) Wu, E. L.; Cheng, X.; Jo, S.; Rui, H.; Song, K. C.; Dávila-Contreras, E. M.; Qi, Y.; Lee, J.; Monje-Galvan, V.; Venable, R. M.; Klauda, J. B.; Im, W. CHARMM-GUI membrane builder toward realistic biological membrane simulations. *J. Comput. Chem.* **2014**, *35*, 1997−2004.
(78) Jorgensen, W. L.; Chandrasekhar, J.; Madura, J. D.; Impey, R. W.; Klein, M. L. Comparison of simple potential functions for simulating liquid water. *J. Chem. Phys.* **1983**, *79*, 926−935.
(79) Berendsen, H. J.; Postma, J. v.; van Gunsteren, W. F.; DiNola, A.; Haak, J. R. Molecular dynamics with coupling to an external bath. *J. Chem. Phys.* **1984**, *81*, 3684−3690.
(80) Parrinello, M.; Rahman, A. Polymorphic transitions in single crystals: A new molecular dynamics method. *J. Appl. Phys.* **1981**, *52*, 7182−7190.
(81) Bussi, G.; Donadio, D.; Parrinello, M. Canonical sampling through velocity rescaling. *J. Chem. Phys.* **2007**, *126*, 014101.
(82) Hess, B. P-LINCS: A parallel linear constraint solver for molecular simulation. *J. Chem. Theory Comput.* **2008**, *4*, 116−122.
(83) Hess, B.; Bekker, H.; Berendsen, H. J.; Fraaije, J. G. LINCS: a linear constraint solver for molecular simulations. *J. Comput. Chem.* **1997**, *18*, 1463−1472.

https://doi.org/10.1021/acssuschemeng.2c06876
ACS Sustainable Chem. Eng. 2023, 11, 1598−1609

(84) Humphrey, W.; Dalke, A.; Schulten, K. VMD: visual molecular dynamics. *J. Mol. Graphics* **1996**, *14*, 33−38.
(85) Kozlovsky, Y.; Kozlov, M. M. Stalk model of membrane fusion: solution of energy crisis. *Biophys. J.* **2002**, *82*, 882−895.
(86) Greenwood, A. I.; Tristram-Nagle, S.; Nagle, J. F. Partial molecular volumes of lipids and cholesterol. *Chem. Phys. Lipids* **2006**, *143*, 1−10.
(87) Sears, V. F. Neutron scattering lengths and cross sections. *Neutron News* **1992**, *3*, 26−37.

https://doi.org/10.1021/acssuschemeng.2c06876
ACS Sustainable Chem. Eng. 2023, 11, 1598−1609